IEEE Access
Multidisciplinary | Rapid Review | Open Access Journal

Received August 14, 2020, accepted September 4, 2020, date of publication September 21, 2020, date of current version October 1, 2020.

Digital Object Identifier 10.1109/ACCESS.2020.3025355

Design and Development of a Battery Powered Electrofusion Welding System for Optical Fiber Microducts

SHAZAD AKRAM, JOHAN SIDÉN, (Member, IEEE), JIATONG DUAN, MUHAMMAD FARHAN ALAM, AND KENT BERTILSSON, (Member, IEEE)
Department of Electronics Design, Mid Sweden University, 851 70 Sundsvall, Sweden

Corresponding author: Shazad Akram (shazad.akram@miun.se)

This work was supported in part by the European Regional Development Fund through the project FIBER.

ABSTRACT At present, optical fiber microducts are coupled together by mechanical types of joints. Mechanical joints are thick, require a large space, and reduce the installation distance in multi-microduct installation. They may leak or explode in the blown fiber installation process. Mechanical joints are subjected to time dependent deterioration under long service times beneath the earth's surface. It may start with a small leakage, followed by damage due to water freezing inside the optical fiber microduct. Optical fiber microducts are made up of high-density polyethylene, which is considered most suitable for thermoelectric welding. For thermoelectric welding of two optical fiber microducts, the welding time should be one second, and should not cause any damage to the inner structure of the microducts that are being coupled. To fulfill these requirements, an LTspice simulation model for the welding system was developed and validated. The developed LTspice model has two parts. The first part models the power input to joule heating wire and the second part models the heat propagation inside the different layers of the optical fiber microduct and surrounding joint by using electro-thermal analogy. In order to validate the simulation results, a battery powered prototype welding system was developed and tested. The prototype welding system consists of a custom-built electrofusion joint and a controller board. A 40 volt 4 ampere-hour Li-Ion battery was used to power the complete system. The power drawn from the battery was controlled by charging and discharging of a capacitor bank, which makes sure that the battery is not overloaded. After successful welding, a pull strength test and an air pressure leakage test were performed to ensure that the welded joints met the requirements set by the mechanical joints. The results show that this new kind of joint and welding system can effectively replace mechanical joints in future optical fiber duct installations.

INDEX TERMS Optical fiber microduct, high density polyethylene, low density polyethylene, IP68, electrofusion welding, electro-thermal analogy, LTspice thermal modeling.

I. INTRODUCTION

Optical fiber technology is the backbone of modern telecommunication systems. The internet revolution has caused a rapid global expansion of fiber-optic networks. In addition to its use in telecommunication, fiber-optic networks are being used for modern fiber-to-the-home and cable TV networks. Along with installations for new users, upgrade of existing fiber-optic networks is also increasing due to increased data traffic demands. Fiber-optic cables are commonly installed in already buried conduits known as microducts [1]. The microducts are made up of high-density polyethylene (HDPE), similar to underground water and gas distribution pipes [2]. When the fiber-optic cables are blown inside already buried microducts, pressurized air is used [3]. A fiber-optic microduct can measure up to 1200 meters, sometimes even more [1], [3]. During installation, it is often necessary to cut and join optical fiber microducts at different lengths. It is also normal practice to bury more than the required optical fiber microducts for future repair and upgrade needs [3].

At present, microducts are joined together by a mechanical type of joint that is exemplified in Figure 1. Mechanical joints can connect one microduct to another microduct of the

The associate editor coordinating the review of this manuscript and approving it for publication was Zhilei Yao.

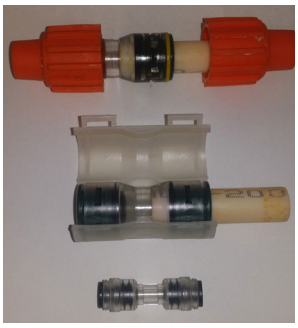

FIGURE 1. Mechanical joint for optical fiber microducts.

FIGURE 2. Straight connector for multi-microduct installation.

same diameter or to a different diameter, and works by the principle of pneumatic push [3]. The insertion diameter of mechanical joints varies from 3.0 mm to 26.0 mm [1], [3]. Inside mechanical microduct joints, there are two metal rings and two rubber O-rings. The metal rings lock to the microduct's surface so that the microducts stay steady in the mechanical joint. The metal rings make the joint withstand a pull strength greater than 200 newtons without breakage. The O-rings sit on the microduct's outer surface and provide protection against air pressure leakage and water seepage. Protection from water is necessary to avoid duct deformation or rupture due to freezing [4]. In order to provide long-time protection against moisture and dust, IP68 protection jackets are commonly installed on each microduct joint as shown in orange color in Figure 1. The mechanical joint can withstand a 15 bar nominal air pressure during blown fiber installation with compressed air. In multi-microduct installations, each microduct pair has to be joined at a different length to keep the overall multi-joint dimeter to a minimum. Straight microduct housings as shown in Figure 2 are normally used, to connect multi-microduct joints, which are cut at different lengths. With the installation of water protection jackets to provide IP68 protection, the installation times are typically between 5 and 15 seconds for each single joint.

Mechanical joints have limitations as they may leak during installation or during service due to O-rings. Like HDPE water and gas installations, the expected service interval for fiber-optic ducts is in the order of decades [2]. O-rings are made of rubber material that loses its elasticity with time. Mechanical joints are bulky and require extra IP68 protection jackets against water and moisture.

To overcome these limitations, thermoelectric welding of fiber-optic ducts is proposed and investigated in this article.

A. HDPE PLASTIC AND ELECTROFUSION WELDING

Plastics are generally divided into two major types [5]. The first type is called thermoset plastics, which are non-weldable plastics. They do not flow under the influence of heat and degrade if excess heat is applied. Typical examples are urea-formaldehyde, melamine-formaldehyde, and phenol-formaldehyde. The second type of plastics is called thermoplastics; they flow when enough heat is applied and are most suitable for welding. Thermoplastics have two subcategories: amorphous and semi-crystalline [5]. Amorphous thermoplastic becomes rubbery when heated and flows under the influence of heat. When cooled down, amorphous thermoplastic becomes hard and brittle. Typical examples are polystyrene and polymethylmethacrylate. Semi-crystalline are partly crystalline and partly amorphous as complete crystallization is never achieved [5]. Examples of semi-crystalline plastics include polyethylene (PE), polypropylene and nylon.

Polyethylenes with densities of 0.910 to 0.925 g/cm^3 are called low-density polyethylene (LDPE); those with densities of 0.926 to 0.940 g/cm^3 are called medium-density polyethylene (MDPE), or sometimes linear low-density polyethylene (LLDPE), whereas those with densities of 0.940 to 0.97 g/cm^3 are called high-density polyethylene (HDPE) [6]. LDPE has a melting point of 106°C to 112°C, MDPE 125 °C, and HDPE 130 to 137°C [7].

As with all polyethylenes, the weathering resistance of HDPE is poor but can be improved by the addition of carbon black or ultraviolet absorbing additives. HDPE is a type of thermoplastic that is most suitable for thermoelectric welding. Depending on the heating method employed, there are about ten or more suitable methods for the welding of HDPE [6]. HDPE is known to be the best material for buried installations due to its low cost, high chemical resistance, and moderate strength properties [8]. HDPE pipes similar to optical fiber microducts are extensively used in water and gas applications worldwide [2]. One of the most popular methods for welding of HDPE pipes in water and gas installations is electrofusion (EF) welding. EF joint welding is based on the method of resistive implant welding [6]. In EF welding, the joule heating effect is usually created by passing alternating current through resistive heating wire.

EF joints are of two types: a tight fit type and a clearance type [9]. In a tight fit type EF joint, there is no clearance between joint and inserted pipes. In clearance type EF joints, there is certain clearance, i.e. less than 2% of the outer diameter of the pipe between joint and inserted pipes [9]. A sketch of a clearance type of EF joint with two pipes inserted from the opposite sides is shown in Figure 3.

The round body of EF joints is usually made up of MDPE or HDPE, and a joule heating wire is wound on the inner side along the inner surface in a helical or a screw thread

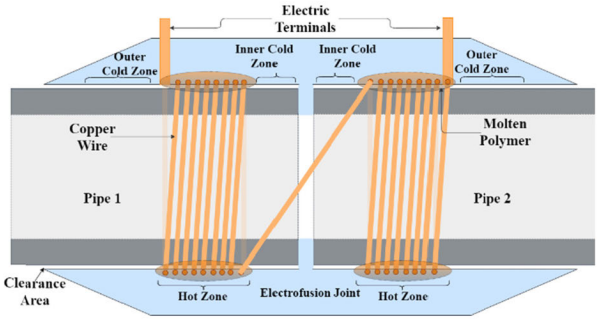

FIGURE 3. Sketch of electrofusion joint.

pattern. Each end of the joule heating wire is connected to the nearest terminal for connection to a power source. When a specified amount of power is supplied at the two terminals, a joule heating effect produces equivalent heat in the copper wire. The heat produced by the copper wire is then conducted to the surrounding plastic. Two heated zones inside the EF joint at equal distance and of equal size on each pipe side are created. When the temperature of the hot zone is raised above the melting temperature of thermoplastic, it melts and eventually liquefies. This molten polymer then flows through the space between the wires towards the pipe. Each hot zone is surrounded by two cold zones to stop the molten polymer from leaking outside the hot zone. After a specified time of the heating cycle, the current is stopped. The interface cools down due to natural convection and the molten polymer hardens again. Thus, a working joint is formed permanently between the EF joint and HDPE pipe interfaces. The voltage range for smaller EF joints starts from as low as 11 volts up to 220v ac, depending on joint size and manufacturer choices [9]. The normal heating time varies from a minimum of 32 seconds for a 25.0 mm EF joint up to several minutes for bigger sizes [6].

For power input to EF joints, specially developed control boxes are used [9]. The control box provides regulated voltage for the required fusion cycle time in accordance with the required energy for fusion. Extensive research has been done on EF welding of HDPE pipe systems for more than five decades [9]. Finite element models and mathematical models have been developed to precisely model the thermal behavior of EF joints [10]–[13]. Nondestructive and destructive methods for EF joint strength estimation and measurement have been developed [14]. Due to the sensitive application of EF joints being used in natural gas transmission systems, a thorough study of the failure modes of EF joints and reasons behind these failures and how to avoid these failures have also been briefly studied in Shi *et al.* [15].

However, despite the success of the EF welding system in water and gas installations, it cannot be directly employed for optical fiber microduct welding due to certain limitations. In EF welding methods developed for water and gas applications, either 110v-220v electricity is directly available through local grid or by using special generators for this purpose. In water and gas EF welding, the energy consumption and time required per joint is not strictly limited. However, in a battery powered handheld optical fiber microduct welding system, there is always a limited battery power, and the time consumed per joint should be short enough to compete with a mechanical joint. The battery-operated system should be able to provide several days of operation without needing to be recharged in remote areas during installations.

In order to successfully replace mechanical joints with EF welding in optical fiber microducts, the heating cycle should be short enough, i.e. around one second. In this very short heat cycle, it should be made sure that the temperature inside the joint reaches higher than the melting temperature of thermoplastics at the welding interface. The energy required to reach the melting temperature should be readily available from a rechargeable Li-Ion battery. In water and gas applications, oxide formation on the HDPE pipe is a major factor in the reduction of overall joint strength [15]. Many scraping tools have been developed to remove outer oxide layers from pipes for EF welding [16]. Moreover, the welded joint should be able to pass the mechanical pull strength test of 200 newtons, and air pressure leakage test of 15 bars.

This article presents a modified EF joint with a controller board for the welding of optical fiber microducts. This new type of optical fiber electrofusion (OFEF) joint has two hot zones and three cold zones on each side. Based on the geometrical shape of the OFEF joint and its material properties, an electro-thermal model of a complete welding system was developed in LTspice. The developed LTspice welding model computes internal temperatures of OFEF joints for a specified power input. The developed LTspice welding model was also validated by measuring actual internal temperatures with a 50μm K-type thermocouples on real OFEF joints. A battery powered controller board was developed, which utilizes a capacitor bank charge-discharge cycle to reduce the OFEF joint load on a 40 volt 4 ampere-hour Li-Ion battery. Three different duty cycles of 30%, 50% and 70% at an output frequency of 80 kHz were used to check the validity of the developed model and complete welding system. The developed OFEF joints were used to weld optical fiber microducts with a power input from the controller board and 40 volt 4 ampere-hour battery. The welded OFEF joints were then tested for pull strength and air pressure leakage for comparison with mechanical joint specifications. Despite the limitation of oxide layer presence, the OFEF joints have passed the conformity tests. The results show a great potential to replace mechanical joints by OFEF welded joints in the future.

B. PREVIOUS WORK

The authors have previously developed and validated an LTspice electro-thermal model of joule heating in high-density polyethylene optical fiber microducts [17]. The developed thermal model was based on thermal to electrical analogy that uses the thermal resistance as electrical resistance and thermal capacitance as electrical capacitance [18]. These thermal parameters like thermal resistance and thermal

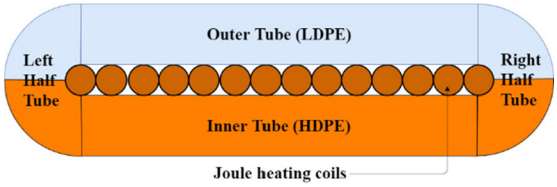

FIGURE 4. Geometric shape of the first layer of 200μm thickness divided into three cylinders along the circumference of the optical fiber microduct.

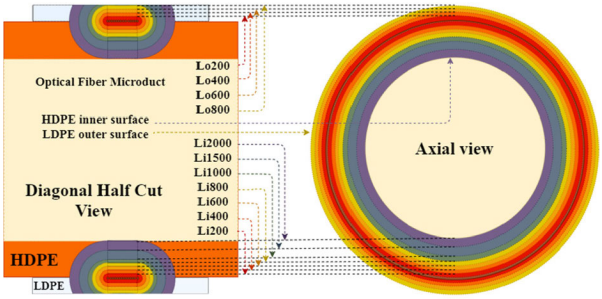

FIGURE 5. Complete layer distribution for thermal modeling of heat propagation inside an optical fiber microduct and the surrounding LDPE sheets.

capacitance were calculated using material properties and geometric shapes [19]. The optical fiber microduct and its surrounding shell were divided into different layers. The geometric shape of the first layer of 200μm thickness, around the joule heating wire consisting of 14 turns of 0.1 mm diameter is shown in Figure 4. Each layer geometry was divided into a total of three tubes or cylinders. Two axial tubes, i.e. inner tube and outer tube, and a third circumferential tube that was further divided into a right half tube and a left half tube.

The complete layer breakdown is shown in Figure 5. It shows five inner layers Li200-Li1000, each 200μm thick, on the inner side of the optical fiber microduct made of HDPE; two inner layers, Li1500 and Li2000, each 500μm thick, on the inner side of the optical fiber microduct made up of HDPE; five outer layers Lo200-Lo1000 of LDPE, each 200μm thick; two outer layers, Lo1500 and Lo2000 of LDPE each 500μm thick, on the outer side of the optical fiber microduct. The thermal resistance $R_{th\ cyl}$ in °C/Watt through the hollow cylinder or tube was calculated by the following formula [20],

$$R_{th\ cyl} = \frac{ln(\frac{r_2}{r_1})}{2 \cdot \pi \cdot \lambda \cdot L} \tag{1}$$

where r_2 is the outer radius and r_1 is the inner radius of the cylindrical wall in meter, λ is the specific thermal conductivity in Watt/°C · meter, and L is the length in meter along the axial direction of tube.

Thermal capacitance C_{th} in Watt · second/°C was calculated using relation [21],

$$C_{th} = c_p \cdot \rho \cdot v \tag{2}$$

where c_p is the specific heat capacity in Joule/Kilogram · °C, ρ is density in kilogram/meter^3, and v is the volume of the material in meter^3. The material properties used for the HDPE layer calculations were $\rho = 950$ Kilogram/meter^3, $\lambda = 0.51$ Watt/°C · meter, $c_p = 2000$ Joule/Kilogram · °C and for LDPE layer were $\rho = 900$ Kilogram/meter^3, $\lambda = 0.36$ Watt/°C · meter, $c_p = 2300$ Joule/Kilogram · °C.

To calculate joule heating wire, thermal resistance R_{thwire} using (1), and thermal capacitance C_{thwire} using (2), the material properties were $\rho = 8940$ Kilogram/meter^3, $\lambda = 397.48$ Watt/°C · meter, $c_p = 376.8$ Joule/Kilogram · °C.

Convection resistance R_{conv} in °C/Watt for the inner layer R_{iconv} and for the outer layer R_{oconv} was calculated using formula [20],

$$R_{conv} = \frac{1}{hc \cdot A} \tag{3}$$

where hc is the convective heat transfer coefficient in Watt/meter^2 · °C and A is the cross sectional area for convection in meter^2. Convective heat coefficient hc was initially chosen to be 28 for the inner layer of HDPE and outer layer of LDPE [7]. Cross sectional area A for convection was calculated by multiplying the respective circumference and length of the convection area. Heat spreading effect inside the layers was considered in the calculation of the convection resistance. As an initial approximation, 45° heat spreading [19] was considered on both sides of inner layer Li2000 and outer layer Lo800. By using (3), R_{iconv} and R_{oconv} were initially calculated to be around $1/(28 \times 9.4 \times 31.6 \times 10^{-6}) = 120.2$ °C/watt and $1/(28 \times 6.0 \times 49.82 \times 10^{-6}) = 119.46$ °C/watt respectively.

Matlab code was used to calculate the individual thermal resistance R_{th} of each inner and outer layer (Rthi200-Rthi2000, Rtho200-Rtho2000), and individual thermal capacitance C_{th} of each inner and outer layer (Cthi200-Cthi2000, Ctho200-Ctho2000). With each layer's calculated thermal resistance and thermal capacitance, a Cauer type thermal network was constructed in LTspice. In the Cauer type thermal model there is a physical correspondence to the material's physical structure inside the device, where the voltage on each node represents the equivalent temperature at that layer [19]. This way, the internal temperatures of the optical fiber microduct made of HDPE and its surrounding layers of LDPE were computed. The thermal properties of HDPE and LDPE materials are not constant in the temperature range 25°C to 180°C [11], therefore the computed LTspice thermal model was optimized to give the best fit for the measured temperatures with 50μm K-type thermocouples [17]. The optimized LTspice thermal model of heat generation and propagation inside the optical fiber microduct [17] is reproduced in Figure 6 [17]. The developed and validated LTspice model shown in Figure 6 has two parts, i.e. the power input part and the thermal model part. The power input part models the input power to joule heating wire, whereas the thermal model part models the resulting temperature at different layers inside the HDPE and LDPE material due

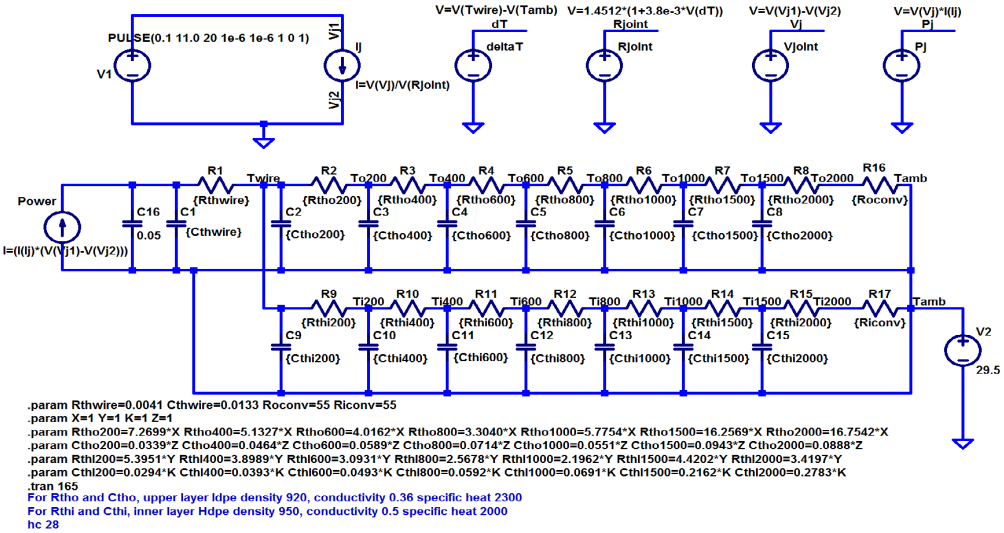

FIGURE 6. Electro-thermal model for heat generation and propagation inside optical fiber microduct.

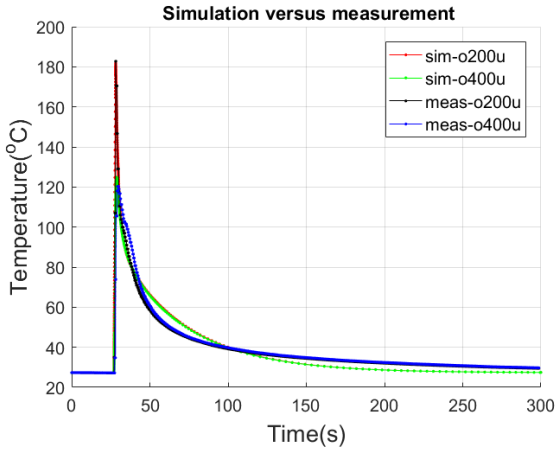

FIGURE 7. Comparison of the LTspice simulation and the measurement results with 71.54 joules input.

to given power input. One of the results of the simulation and validation experiment in [17], with a power input of 13.2 volt × 5.42 ampere = 71.54 watts, is reproduced here in Figure 7. In Figure 7, the red curve, i.e. sim-o200u, is the thermal response of the simulation at the first 200μm thick LDPE outer layer as shown in Figure 5, whereas the black curve, meas-o200u, is the actual measured response of the first 200μm thick LDPE outer layer with the 50μm K-type thermocouple. Similarly, sim-o400u is the simulation result, and meas-o400u is the measured result of the second outer layer of 200μm thickness. Figure 7 clearly shows that a temperature of 182°C was achieved with an input power of 71.54 joules.

II. OPTICAL FIBER ELECTROFUSION (OFEF) WELDING SYSTEM DESIGN AND DEVELOPMENT

Based on the thermal modeling theory and methods presented in Akram *et al.* [17] and shortly described in the previous section, a new type of OFEF joint and its complete welding system was modeled in LTspice. Simulation results of the LTspice welding model were used to fabricate prototype OFEF joints and their controller board.

A. PRELIMINARY TEMPERATURE ESTIMATION OF THE OFEF JOINT

In the validation experiments of Akram *et al.* [17], 14 turns of 0.1 mm diameter copper wire were wound as joule heating wire. If this same wire is wound on each side of the EF joint shown in Figure 3, it becomes a direct transformation of the experimental results shown in Figure 7. When turns of joule heating wire are doubled and the corresponding input voltage is also doubled, i.e. to 26.4 volts, the same temperature of 182°C will be reached by using $71.54 \times 2 = 143.08$ joules according to the results shown in Figure 7.

B. PRELIMINARY BATTERY POWER ESTIMATION

The available battery power is theoretically about 40 volt × 4 ampere-hour = 160 watt-hour = 576000 Joules. The battery weight was approximately 960 grams. The battery was selected to give high enough energy for welding, which was also suitable for use in handheld welding equipment.

This article shows that 287.43 joules are required with maximum energy losses to weld a 14.06 mm diameter optical fiber microduct that can pass the pull strength and air pressure tests. Theoretically, in such cases, a fully charged 40 volt 4 ampere-hour battery is capable of powering 2004 OFEF joints.

C. PRELIMINARY WELD STRENGTH ESTIMATION

As mentioned earlier, the normal heating time for EF joints used in water and gas installations is about 32 seconds for a 25.0 mm EF joint [6]. This time allows the molten polymer to flow and fill the space between the pipe and joint interface.

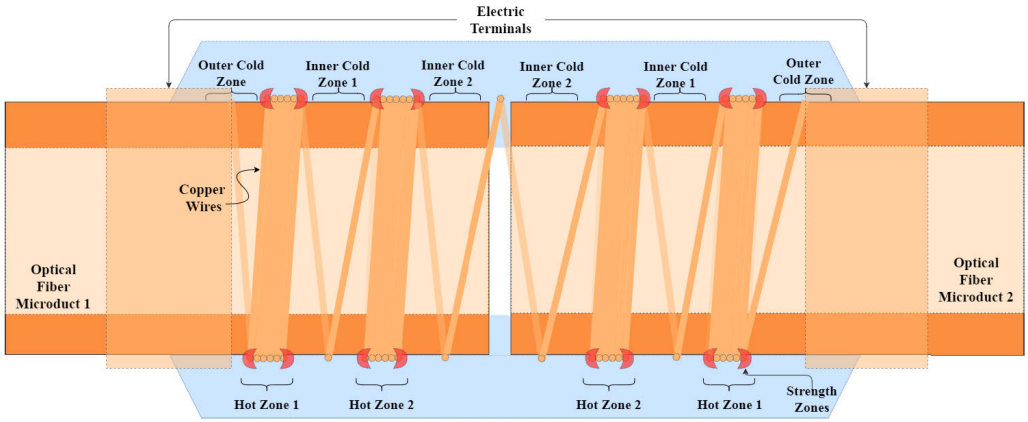

FIGURE 8. Mixed winding pattern of $6+1+6+1+1+6+1+6=28$ turn wire winding.

As a requirement to compete with a mechanical joint for quick heating within one second, there is not much time to allow molten polymer to flow through copper wires and fill the clearance area as shown in the clearance type EF joint in Figure 3. Therefore, a tight fit design is a preferred technique for welding of optical fiber microducts.

In validation experiments conducted by Akram *et al.* [17], the total width of the melt zone or fusion zone was about 1.6 mm wide across the circumference of the optical fiber joint, i.e. 1.4 mm for 14 turns of 0.1 mm diameter joule heating wire and 0.1 mm heat spreading on both sides of the wire. The 1.6 mm wide fusion zone was selected based on a preliminary assessment indicating that due to oxidation and other EF joint strength degrading factors described in Shi *et al.* [15], the resulting weld may degrade up to 50% in strength. In this case, only an effective fusion area of 0.8 mm wide (50% or half of 1.6 mm) along the circumference of the optical fiber microduct will give the joint's actual strength. For this reason, it was assumed that the effective joint with 50% strength will be 0.8 mm wide on each side, which in turn will be equal to the strength of the joint's wall thickness, which is also 0.8 mm thick, i.e. four layers of 200μm each. This means that the weld strength will be equal to the wall strength of the OFEF joint, which is a preliminary estimation because the strength of the OFEF joint has not yet been measured; it may or may not pass the strength test requirements of 200 newtons. Depending on the required strength of the OFEF joint, the width of the fusion zone may need to be increased more than 1.6 mm on either side, which in turn will require more energy to melt more deeply inside optical fiber microduct's surface for a stronger joint.

The joint wires can be wound in two patterns. In the first pattern, they can be wound as a normal EF joint wire with a fixed space between two adjacent turns as shown in Figure 3. This type of winding is possible for bare wires with no insulation coating. During a short heating cycle of one second for optical fiber microduct welding, if the space between the wires is not completely melted for any reason, then during the air leakage test, air may leak in a circulating pattern inside the space between the wire turns and eventually leak from the joint ends. Thus, the whole joint becomes void. In the second pattern, they can be wound as a tight wire winding with literally no space between two adjacent turns, as shown in Figure 4. This type of winding is only possible with insulation-coated wires.

The mechanical strength of the EF joint depends on the polymer to polymer molecular diffusion [6], [9]. In the case of a tight winding pattern, the joint strength will only be dependent on both side ends of the winding, i.e. the right half and left half of the tube as shown in Figure 4. The outer LDPE layer will have no direct contact with the inner HDPE layer as in Figure 4, and will not contribute significantly to the weld strength of the OFEF joint.

To overcome the problem of circulating air leakage between the joule heating wires and reduced joint strength in a tight winding pattern, a mixed pattern wire winding was utilized in the development of the OFEF joint. For a 2.9 ohm resistance joint, 14 turns single hot zone winding on each side, was split into two hot zone windings on each side. This way, two heating zones inside three cold zones on each side of the OFEF joint were created as shown in Figure 8. Two hot zones give better air leakage protection as well as better mechanical pull strength. The wire winding pattern shown in Figure 8 is $6+1+6+1=14$ turns on one side, with an equal but opposite pattern of this sequence, i.e. $1+6+1+6=14$ turns on the second side, to achieve symmetry in the OFEF joint and respective fusion zones.

D. WELDING MODEL

Fujikake *et al.* [12] stated the basic temperature requirements for the EF joint as:

1) The minimum value of interface temperature between the HDPE pipe and the EF joint has to be larger than 160°C.
2) The maximum PE temperature around the heating wire has to be lower than 350°C to prevent PE degrading near to the wire.

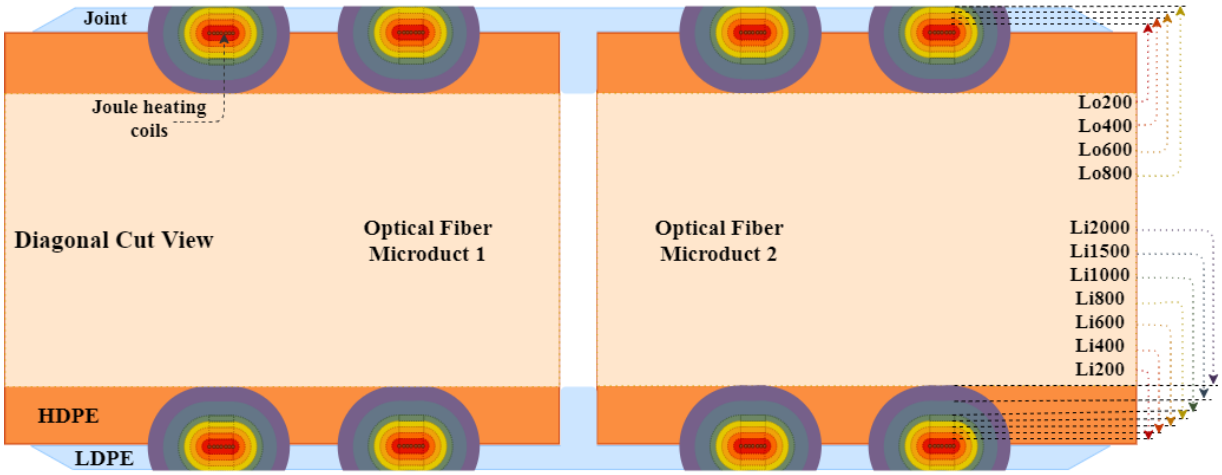

FIGURE 9. Complete geometric layer distribution of heat transfer in the optical fiber microduct and joint.

3) The maximum temperature of the pipe's inner wall has to be lower than 110°C to keep the stiffness of the pipe and avoid thermal damage.

From the results of the validation experiments performed in Akram *et al.* [17], it can be concluded that all three conditions stated above can be very easily met if the temperature at the first outer layer of 200μm (Lo200 in Figure 9), is kept around 190°C. These results can be directly adopted for the development of the OFEF joint welding system because they have the same material and number of layers with a similar geometric structure in both cases. The only difference is the width of the heating zone, which is split into half on each side. Therefore, in the following sections of this article, the temperature on Lo200 is used as a benchmark to check the validity of the OFEF joint against temperature requirements.

In the validation experiments performed in Akram *et al.* [17], a variable DC power supply, TTi CPX400A, was used. For the design of a battery powered welding system, the battery's rated output voltage and output current, put certain limitations on the energy available for welding. If a 2.9 ohm joint is connected directly to a 40 volt 4 ampere-hour battery, it will initially draw around 13.79 amperes of current at the start of the heating cycle. This current of 13.79 amperes will put undesirable load on the battery and may damage the battery during short term or long term usage. In order to limit the power input from the battery to a 2.9 ohm OFEF joint, a capacitor bank utilizing pulse width modulation (PWM) based charge discharge heating technique was adopted. The capacitor bank can provide the required extra energy at the start of the heating cycle until the resistance of the joint increases due to joule heating and limit the power drawn from battery. According to Bowman [9], it is also important that the energy is deposited within the EF joint as quickly as possible. By doing so, the energy is initially localized at the fusion interface, thus increasing the interface temperature to a higher value for a given energy input. The use of a capacitor bank also increases the quick deposit of energy inside the joint within a given time due to a higher amount of current available.

Based on the theory and methods in Akram *et al.* [17], which are shortly described in the *PREVIOUS WORK* section of this article, an LTspice model for a complete welding system was developed and validated. The developed LTspice welding model is shown in Figure 10. The welding model consists of two parts: the power input part and the heat propagation part. The power input part took into account the PWM switching and charge-discharge cycle of a capacitor bank. The total capacitance of 0.0562 farads, i.e. 17 capacitors of 3300μf each, which can store about 34.4 joules of energy at 35 volts, was used to model the power input section. By adding the capacitor bank, the welding system can easily provide 194.5 joules of energy. By changing the PWM duty cycle, the charging and discharging of a capacitor bank, and hence power input to the joint, can be easily controlled. This way, by changing PWM duty cycle, it is possible to vary the required temperature at the desired layer during the heating cycle. To model the heat propagation part, a mixed winding pattern, shown in Figure 8, was utilized to develop the thermal model of the OFEF joint welding. The layer distribution for two heating zones on each side of the OFEF joint is shown in Figure 9. For simplicity, 7 turns, i.e. 6 + 1 turn of joule heating wire, were used to model a single heating zone. Matlab code developed and validated in Akram *et al.* [17] was used to calculate the thermal parameters of a single heating zone. Calculated thermal parameters of a single heating zone were connected in parallel to model the four complete heating zones of the OFEF joint. This was done by changing the multiplying variable X and Y by 0.25, since resistance in parallel decreases by a factor of four. Similarly, variables K and Z were multiplied by 4, as capacitance in parallel increases by a factor of four.

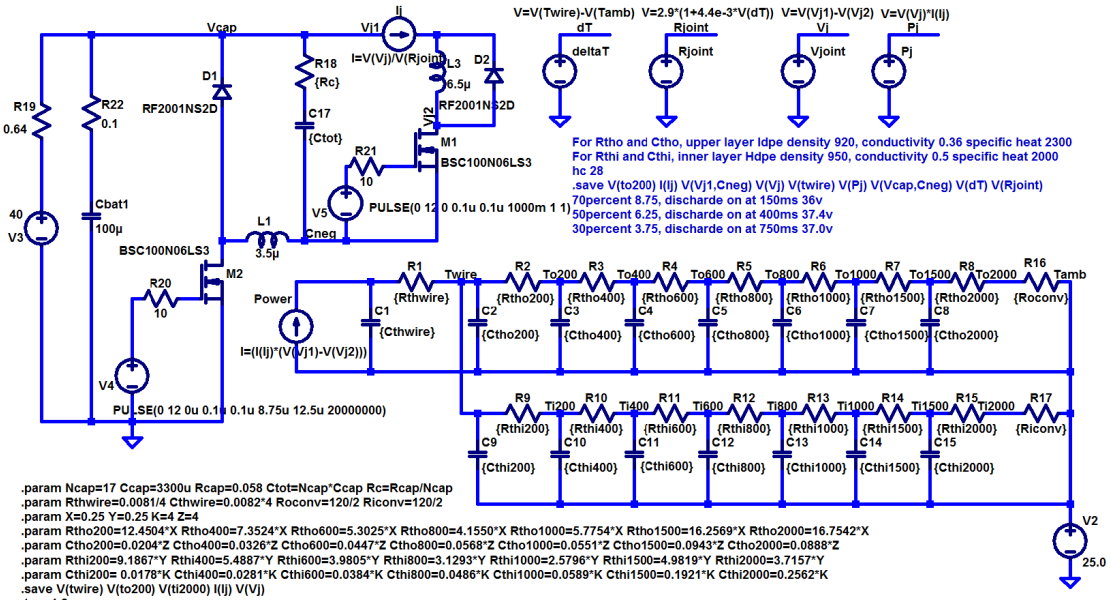

FIGURE 10. LTspice welding model for optical fiber microduct joints.

The welding model shown in Figure 10 can be used to compute the effect of a capacitor bank, required current and voltage to reach a certain temperature at a desired layer depth inside the OFEF joint and optical fiber microduct. In the LTspice welding model shown in Figure 10, the voltage ''V(twire)'' at node ''Twire'' gives the expected temperature of joule heating wire in volts; the voltage at node ''To200'' is the expected temperature on the first 200μm outer layer, i.e. Lo200 as shown in Figure 9. Similarly, the voltage at ''Ti2000'' is the expected temperature in volts at the inner wall of the optical fiber microduct exactly under the heating wire, i.e. Li2000 in Figure 9. For simulation, the initial voltage on the capacitor bank was set to 35 volts, which corresponds to a fully charged capacitor bank, and only the benchmark voltage V(to200) was computed. Three separate simulations were done with a 30%, 50%, and 70% duty cycle at a switching frequency of 80 kHz. The LTspice simulation of 30 seconds took around 160 hours for all three duty cycles running in parallel. The results of the simulations show the power input for joule heating wire for each duty cycle, which is presented in Figure 11. Their corresponding temperatures at the first outer layer Lo200, are presented in Figure 12, i.e. V(to200)-PWM, with a green waveform.

Due to the limitation of the very long LTspice simulation time and limited memory available to store simulation data on a PC, a second simulation model was developed by replacing the PWM and capacitor bank, as shown in Figure 10, with a DC power input source similar to the one used in Figure 6. The equivalent DC welding model is shown in Figure 13. In the equivalent DC welding model, the input power was supplied as a DC step input voltage, which was equal to the average input voltage as shown in Figure 11. The equivalent DC welding model of Figure 13 had a simulation time of about one second, as compared to the very long simulation time required for the welding model in Figure 10. Moreover, in the equivalent DC input model, it is very easy to adjust other variables, like room temperature (V2), and compute temperature on other layers like V(ti2000) and V(twire). Three simulations were done with input voltages equal to the average input voltages shown in the results of Figure 11. The resulting node voltages V(to200) are plotted again in Figure 12, i.e. V(to200)-DC, with blue waveform, along with results obtained by the PWM input for node voltage V(to200).

E. DEVELOPMENT OF OFEF JOINT SAMPLES

A proper EF joint is preferably manufactured using an injection molding technique [7], [12], [22]. At an initial stage to validate the simulation results shown in Figure 11 and 12, an in-house prototype OFEF joint was fabricated on an aluminum mold as pictured in Figure 14. The outer diameter of the aluminum mold was 14.06 mm, which was equal to the outer diameter of the optical fiber microduct. For fabrication of the prototype OFEF joint, a single 100μm thick LDPE layer was wound on an aluminum mold and then two rings made of copper polyethylene sheet were placed at each end of this LDPE layer. The copper rings were used as power input terminals instead of the pin-like power terminals used in water and gas EF joints. Copper ring connectors can give a faster connection with the controller board by using two round clamp connectors, which will sit firmly around the copper rings inside a prototype welding machine, as shown in Figure 15.

For joule heating, six turns of a 0.1 mm diameter wire for the first hot zone, followed by one turn to the second hot zone was wound. Then six turns to the second hot zone with one turn to the middle of the joint was wound. The

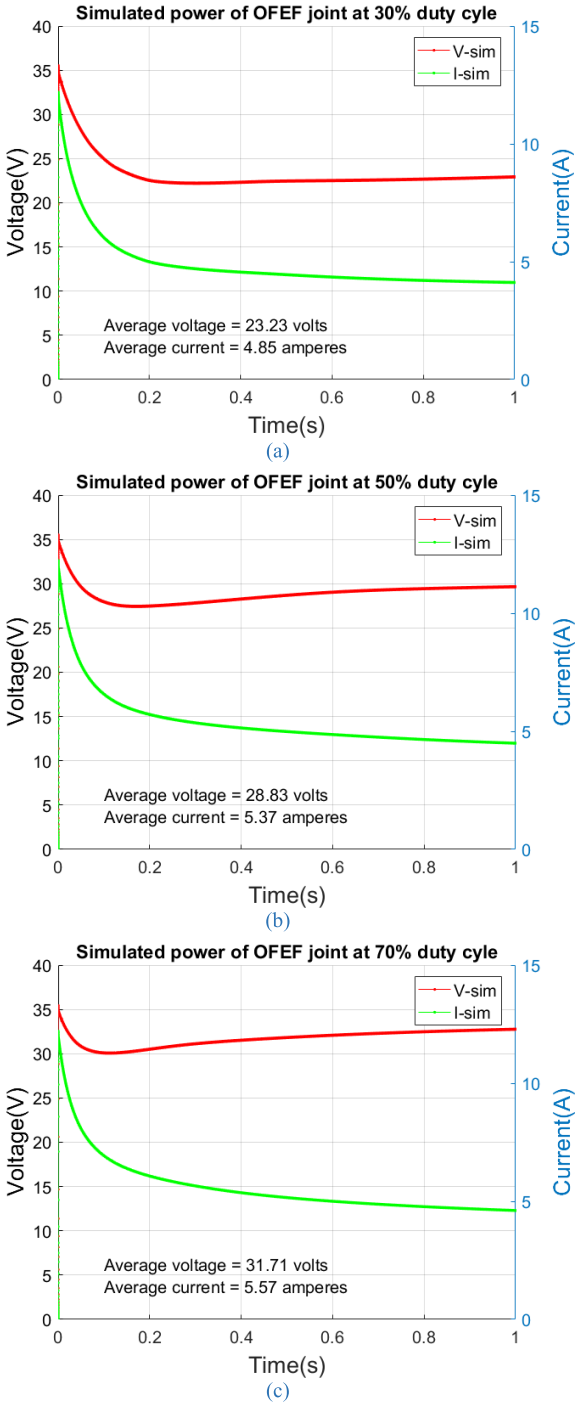

FIGURE 11. Simulated power dissipation of the OFEF joint with 30%, 50% and 70% duty cycles.

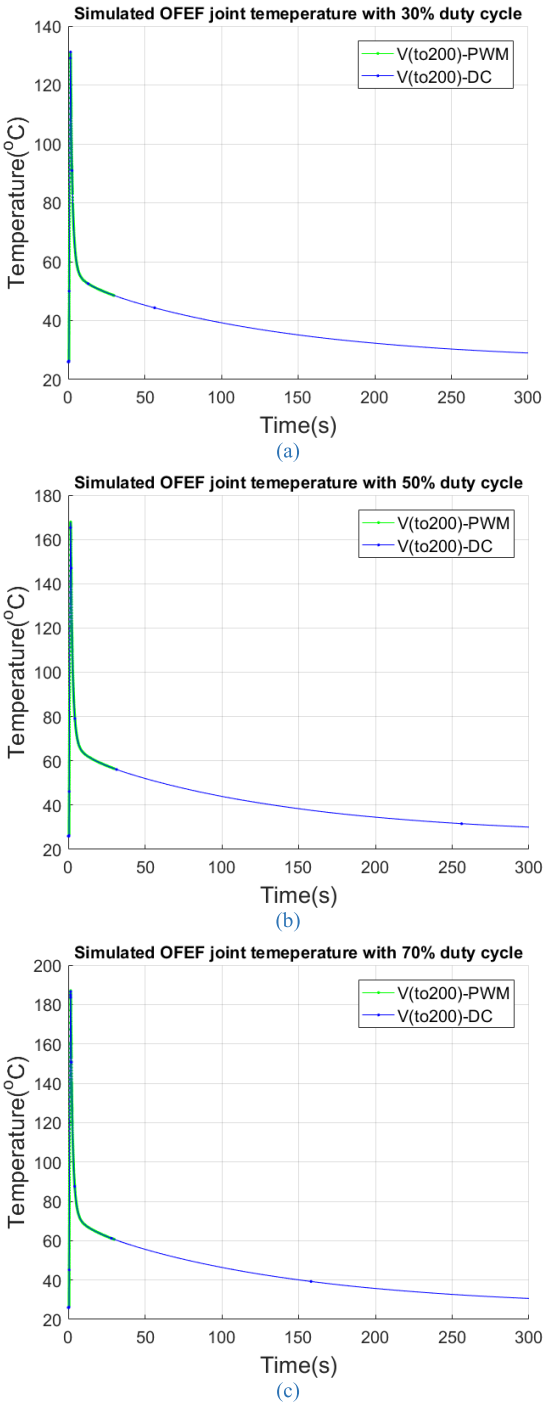

FIGURE 12. Comparison of the simulated voltage V(to200) of the OFEF joint with 30%, 50% and 70% duty cycles PWM inputs and equivalent DC power inputs.

same sequence was repeated for the other half in the opposite pattern. Starting from the middle one turn to the second hot zone of six turns, and then again one turn to the first hot zone on the other side, which finished on the opposite side copper ring. A mixed winding pattern of $6 + 1 + 6 + 1 + 1 + 6 + 1 + 6$ turns as shown in Figure 8 was followed. This method created two hot zones within three cold zones on each side of the OFEF joint. After the winding of the joule heating wire, a 200μm thick LDPE layer was wound and a 50μm K-type thermocouple was placed at that layer (the same as Lo200 in Figure 9). These 50μm thermocouples are not available off the shelf. The lower mass of thermocouple beads provides a faster temperature response [20]. These thermocouples were custom-built for faster temperature response measurement with a Picolog TC-08 data logger. In total four

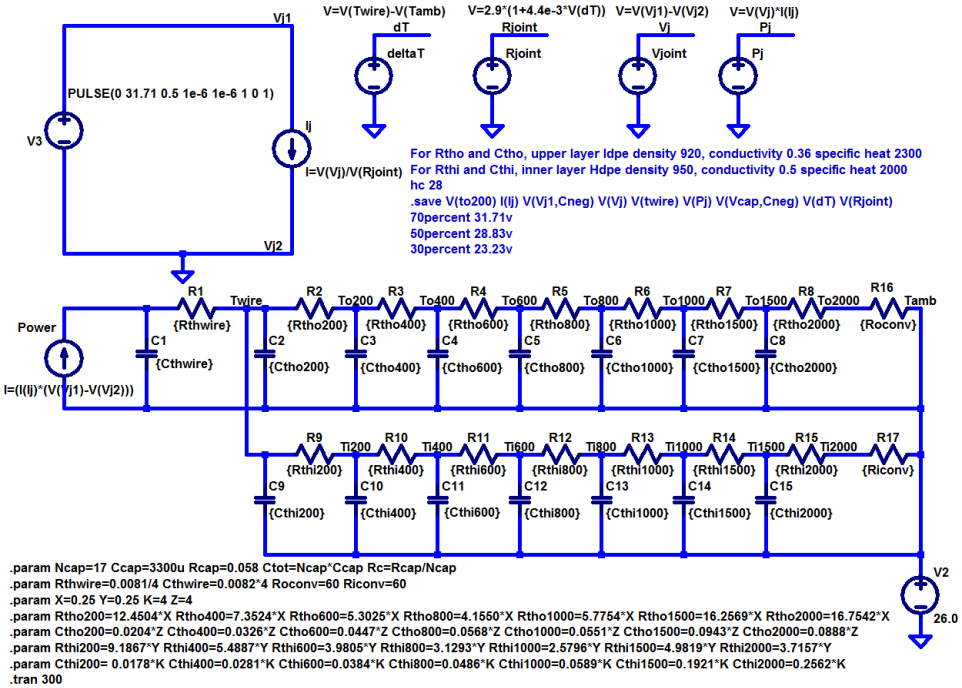

FIGURE 13. Equivalent DC input welding model for faster simulation in LTspice.

FIGURE 14. Fabricated optical fiber microduct electrofusion joint with mold.

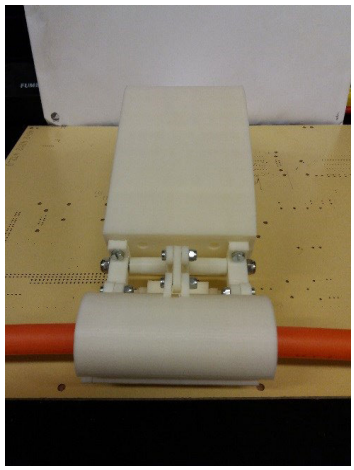

FIGURE 15. Prototype OFEF joint welding machine.

200μm LDPE layers were wound. By carefully monitoring the sample temperature with a Fluke Ti9 thermal imager, the OFEF joint sample was heated with a hot air gun up to 130°C, such that all its layers diffused and provided a good mechanical strength. The OFEF joint sample was then cooled down by submerging it into a water container for 5 seconds, which was kept at room temperature. The sample was then air cooled until it reached near to room temperature. After cooling down to room temperature, the prototype OFEF joint was carefully removed from the aluminum mold. In total 24 prototype OFEF joints were fabricated with a similar method, half with thermocouples, and half without thermocouples. OFEF joints with thermocouples were used for validation of the power and temperature simulation results shown in Figure 11 and 12. OFEF joints without thermocouples were used for pull strength tests, air pressure leakage and water seepage tests.

F. DEVELOPMENT OF CONTROLLER BOARD

In order to validate the results of the simulations, a prototype controller board was fabricated and programmed. The block diagram of the controller board is shown in Figure 16. A 40 volt 4 ampere-hour battery was used to power the whole system. The input voltage of the battery was

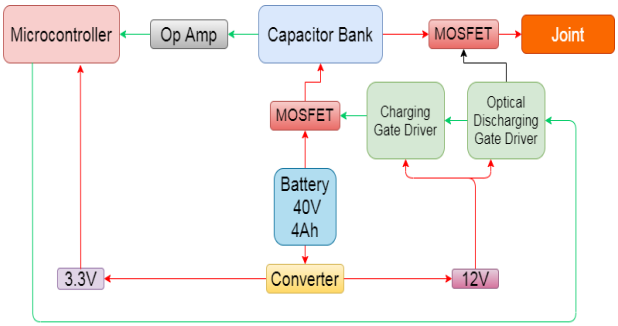

FIGURE 16. Block diagram of the controller board for the OFEF joint welding system.

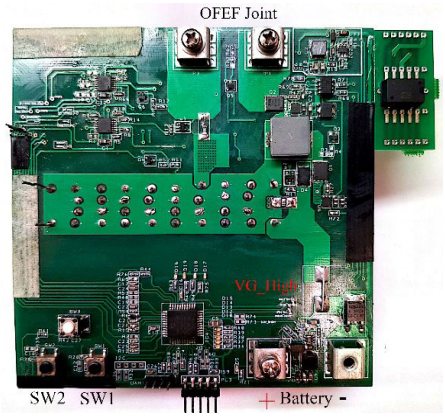

FIGURE 17. Developed controller board with capacitor bank on the opposite side.

converted to 3.3 volts for power supply to the microcontroller and 12 volts to the driver circuit of charge and discharge MOSFETs. The charging MOSFET charges the capacitor bank according to the PWM supplied by the microcontroller. The discharging MOSFET discharges the capacitor bank and battery power across the OFEF joint. The manufactured controller board along with the microcontroller and a capacitor bank on the opposite side is shown in Figure 17.

The controller board utilizes the DsPIC33FJ16GS404 microcontroller for the welding operation and welding time and duty cycle settings at a programmed frequency of 80 kHz. When switch SW2 (bottom left on the PCB) is pressed, the microcontroller charges the connected capacitor bank until the voltage on the capacitor bank reaches a threshold of 35 volts. When the discharge button SW1 (bottom right on the PCB) is pressed, the microcontroller turns on the discharge MOSFET and capacitor energy is discharged across the OFEF joint while the charging MOSFET is running on a set duty cycle.

III. VALIDATION TESTS OF THE OFEF WELDING SYSTEM

The complete validation of the OFEF welding system consists of two parts. In the first part, the simulation results of the LTspice welding model are validated. In the second part, the test of the welded OFEF joint was performed with the pull strength test and air pressure leakage test.

TABLE 1. Equipment and software for validation.

Equipment	Model/Status
OFEF joint samples	With and without diffused 50µm K-type thermocouples
Controller board	As shown in Figure 17
Battery	40 volts 4Ah Li-Ion Fully charged
Current probe	Agilent N2782B with N2779A PSU
Voltage probe	Picolog TA058
Oscilloscope	Rohde and Schwarz RTM1054
Thermal data logger	Picolog TC-08
Programmer	PICkit 3
PC or Laptop	Installed MPLAB X IDE v5.05 and Picolog 6 software

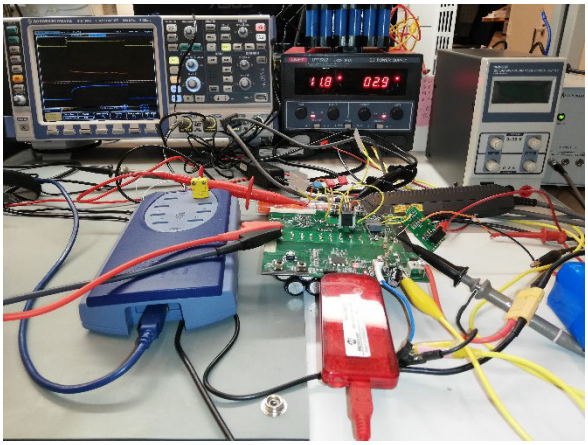

FIGURE 18. Measurement setup for validation of simulated power and temperature of the OFEF joint welding system.

A. VALIDATION OF THE WELDING MODEL WITH THERMOCOUPLE MEASUREMENTS

Table 1 shows the list of equipment and software used to validate the simulated results shown in Figure 11 and 12.

VALIDATION PROCEDURE:

1) Connect the OFEF joint sample with copper wires to the output terminals of the controller board.
2) Connect the diffused thermocouples of the OFEF joint to the input of the Picolog TC-08 thermal data logger.
3) Connect Keysight current probe N2782B to the output current wire of the controller board, connected to the OFEF joint.
4) Connect the Picolog TA058 differential probe to the two power connector wires of the OFEF joint.
5) Connect the output terminal of the Keysight current probe N2782B and Picolog TA058 differential voltage probe to the Rohde and Schwarz RTM1054 oscilloscope.
6) Connect the trigger probe of the oscilloscope to the VG-High pin of the controller board with a 120 ohm resistance in series. VG_High is the driving signal of

the discharge MOSFET, which acts as a trigger source for the oscilloscope.

7) Connect the PICkit 3 to the UART data pins of the controller board as shown in Figure 18.
8) Connect the provided 40 volts 4 ampere-hour battery to the power input terminal of the controller board.
9) Connect the USB terminal of the Picolog TC-08 data logger and USB terminal of the PICkit 3 programmer to a PC or laptop with MPLAB X IDE v5.05 and Picolog 6 software installed and configured.
10) Start MPLAB X IDE and program the DsPIC microcontroller for the desired duty cycle for charging, discharging, and time for welding.
11) Start the Picolog 6 software and configure it for the correct terminal and thermocouple type. Start recording.
12) Press SW2 on the controller board and when the capacitor bank is charged to 35 volts, Led D18 will be turned ON indicating that the controller board is ready for welding.
13) Press SW1 and the capacitor bank will be discharged across the OFEF joint while the charging MOSFET will be running at the programmed duty cycle and the discharge MOSFET will be completely ON.
14) With the VG_High pin turned ON, the connected oscilloscope will trigger and capture the voltage and current across the OFEF joint.
15) The Picolog 6 will capture the temperature curve at the desired layer in the OFEF joint.
16) After a programmed welding time of one second, the charge and discharge MOSFETs will be turned off.
17) Wait for at least 300 seconds for the Picolog 6 software to capture the cooling curve due to natural convection at room temperature.
18) Stop the Picolog 6 temperature recording after the 300-second cooling cycle.
19) Save the captured voltage, current, and temperature data.

This is how the three different duty cycle settings of 30%, 50%, and 70% at a frequency of 80 kHz were used to measure the temperature at layer Lo200 of the OFEF joint samples. A comparison of the digitized waveforms of the measured voltage and current across the OFEF joint, with simulated waveforms of voltage and current for each duty cycle, are presented in Figure 19. The comparison of the measured and simulated temperature for each respective duty cycle is presented in Figure 20.

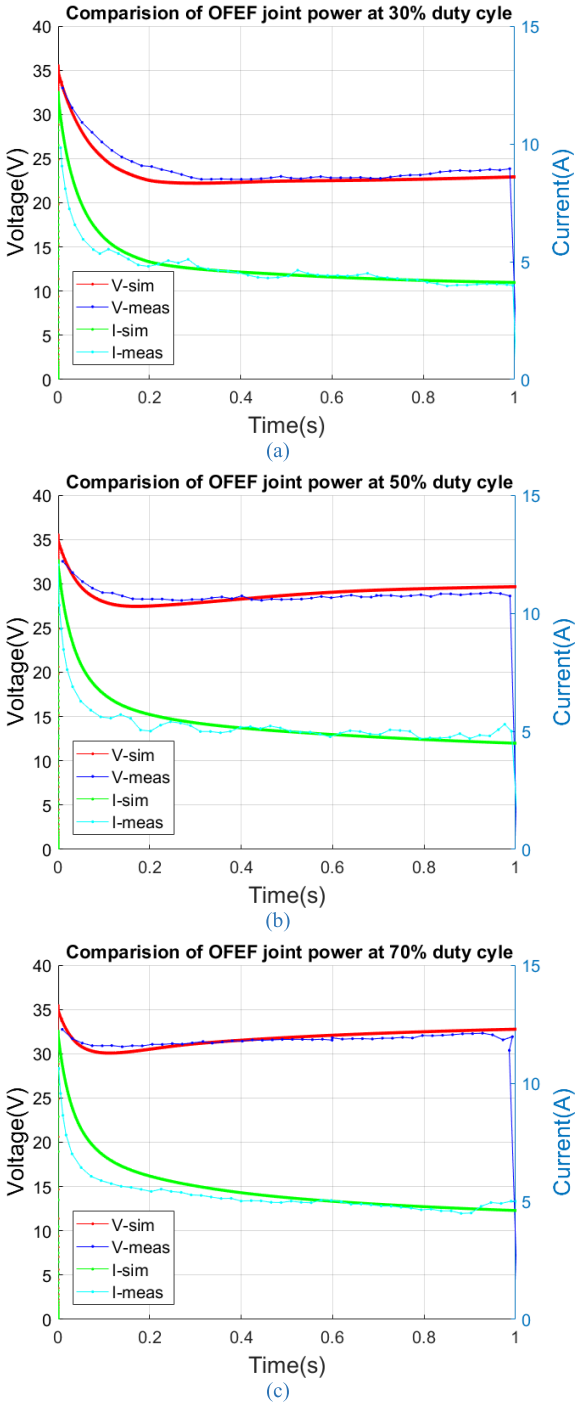

FIGURE 19. Comparison of simulated and measured power applied to the OFEF joint.

B. LAYER MELT TEST

The layer melt test provides a visual inspection of the physical melting inside the OFEF joint at the layer level. Three separate samples were made for this purpose. For each sample, 28 turns of a 0.1 mm copper wire in a 6+1+6+1+1+6+1+6 turn pattern were wound on three different HDPE optical fiber microduct samples. On each of these samples four layers of LDPE sheet, each one 200μm thick, were wound and sealed on the outer side with a soldering iron. Three different duty cycles of 30%, 50%, and 70% at 80 kHz from the controller board were used to melt the LDPE layers inside the three samples for a one-second heating cycle. After completing the heating cycle, all three samples were unwound layer by layer. These samples were not preheated like the OFEF joints. It was

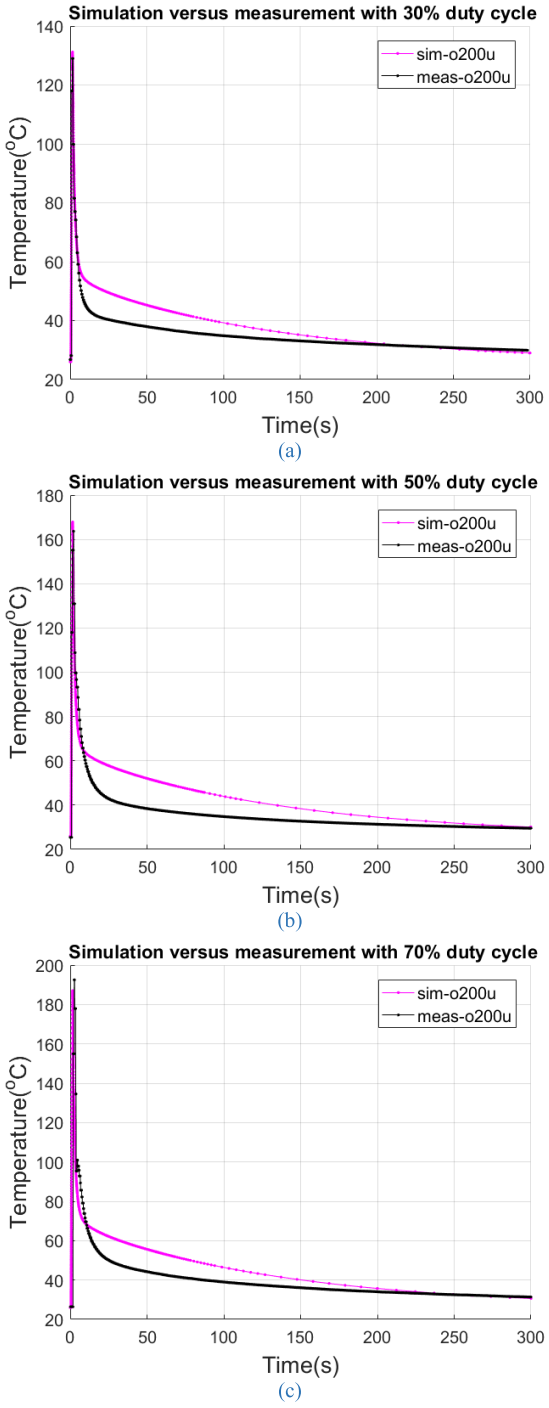

FIGURE 20. Comparison of simulated and measured temperature at the first 200μm thick OFEF joint layer.

easy to unwind the LDPE layers where the heat had not been enough to completely melt the LDPE layer exactly above the melting zones. When a melted hot zone layer was reached, it became difficult to peel off the upper LDPE layer while avoiding damage to the LDPE layer underneath. It can be seen that these layers were effectively melted and it was not possible to separate them. The results of the layer peeling are shown in Figure 21. It can be seen that melting with a 70%

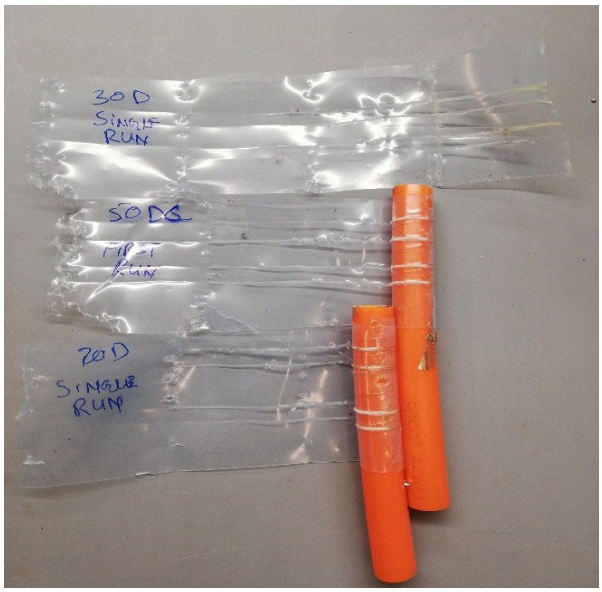

FIGURE 21. Layer melt test showing melted layers of 200μm LDPE with 30%, 50% and 70% duty cycles.

duty cycle was enough to completely melt the hot zones of the first two layers (Lo200-Lo400). Heating with a 50% duty cycle melted nearly a quarter less of two layers of hot zones while a 30% duty cycle only melted the hot zones of the first layer.

C. PULL STRENGTH TEST

To measure the pull strength, the samples of the OFEF joints welded with 30%, 50%, and 70% duty cycles were connected to Mecmesin MultiTest 2.5-dV with a AFG 2500N pull strength testing machine. One end of the two welded microducts was connected to the base on the Mecmesin MultiTest 2.5-dV machine and the other to the hook of the AFG 2500N calibrated strength meter as shown in Figure 22. The two sides of the welded microducts were pulled apart with the machine until either the OFEF joint weld broke away from microduct's outer surface, or when the OFEF joint wall broke due to excessive pull strength. The OFEF joint wall breaks when the welded part of the OFEF joint, i.e. the melted hot zones, remains welded on the microduct surface, but its wall tears apart from the middle due to applied force.

D. AIR PRESSURE LEAKAGE TEST

To perform the air pressure leakage test, one end of the welded OFEF joint sample was melted with a hot air gun to completely seal it. The other end of the sample was connected to the air compressor's nozzle, which could provide a maximum of 10 bars of air pressure as shown in Figure 23. The air pressure was increased gradually in steps of 2 bars at a time. At first, 2 bars were set on the compressor, and the sample was immersed in a mixture of dishwashing liquid and water to inspect any leakage. When no leakage was found, the pressure was increased by another 2 bars, and so on, until either air

FIGURE 22. OFEF joint sample for test on Mecmesin MultiTest 2.5-Dv.

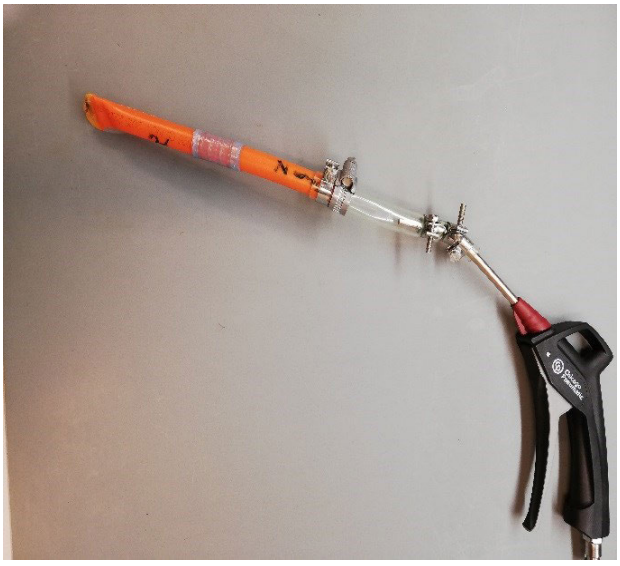

FIGURE 23. OFEF joint sample prepared for air pressure test.

leakage was detected or the compressor reached its maximum rated output of 10 bars. The process was repeated for each sample welded with a 30%, 50%, and 70% duty cycle.

IV. RESULTS AND DISCUSSION

The results of this study are discussed separately in the following.

A. RESULTS OF THE POWER COMPARISON

As the results in Figure 19 shows, the measured input voltage and current waveforms are quite close to the simulated input

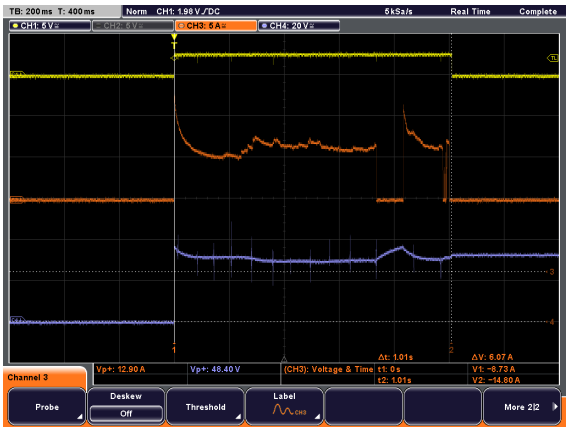

FIGURE 24. OFEF joint voltage and current spikes, as well as fusing with an 80% duty cycle.

voltage and current waveforms of an OFEF joint. Due to tolerances in sample preparations, tolerances in measurements, and changes in the physical behavior of the materials during heating [17], a complete match between simulation and validation measurement could not be achieved. In simulations, mostly ideal components were used, and their output response was much smoother than the physical components used in validation experiments. The summary of the average simulated and average measured power consumption of the OFEF joint, with 30%, 50%, and 70% duty cycles, is presented in Table 2. The maximum difference between average measured and average simulated power consumption for three duty cycles in Table 2 is around 5%. This difference in simulated and measured power can be due to manufacturing tolerances in the OFEF joints and their physical behavior during the heating cycle.

The OFEF joints used for measurements were custom-built. It was observed that despite all the care, the custom-built OFEF joints have had air trapped between layers, which was difficult to avoid. When this trapped air was present near the joule heating wire, it generated undesired spikes in current and voltage waveforms. This fact was more obvious at higher duty cycles. Voltage and current consumption of one sample of OFEF joint, tested with an 80% duty cycle, are shown in Figure 24. It shows that the voltage and current waveforms demonstrate spikes, and eventually the OFEF joint fuses at around 720 milliseconds, and then again starts conducting at 820 milliseconds. These spikes in power consumption are due to a small amount of air, which causes a make-break contact between the wire and its surrounding LDPE layer. This fact in turn changes the temperature of that specific part of joule heating wire and hence its resistance. This uncontrolled change in wire resistance during the heating cycle causes the difference in power consumption of each OFEF joint sample. Due to the risk of joule heating wire fusing, a maximum 70% duty cycle was used in validation experiments. If OFEF joints are manufactured using injection molding techniques [7], [12], [22], such that the area around the joule heating wire is completely covered with molten

TABLE 2. Comparison of the average power consumption of the OFEF joint.

Duty Cycle	Simulation	Measurement
30%	23.23V×4.85A=112.66J	23.42V×4.69A=109.84J
50%	28.83V×5.37A=154.81J	29.03V×5.24A=152.11J
70%	31.71V×5.57A=176.62J	31.77V×5.28A=167.74J

FIGURE 25. A diffused K-type thermocouple inside an OFEF joint sample.

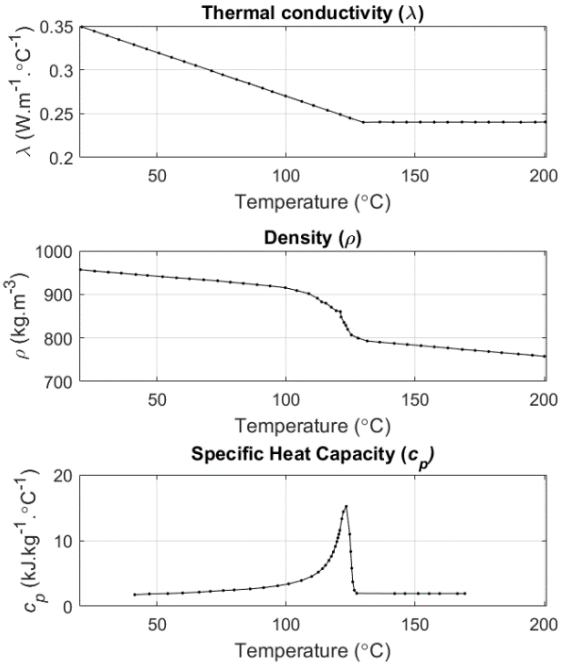

FIGURE 26. Thermal properties of polyethylene.

polyethylene, then voltage and current spikes can be minimized and a smaller variation in average power consumption is expected.

B. RESULTS OF THE TEMPERATURE COMPARISON

The comparison between the simulated and measured temperature in the OFEF joint is shown in Figure 20. As can be seen, there is a good match between the peak simulated and peak measured temperatures on layer Lo200. At a 30% and 50% duty cycle, the peak measured temperature is lower than the peak simulated temperature, while at a 70% duty cycle it is opposite. The magnified view of 50μm thermocouple placed on the joule heating wire is shown in Figure 25. During sample preparation, the preheating of the OFEF joint can diffuse 50μm thermocouple on either side of the neighboring layers. This factor is uncontrollable with the present method of OFEF joint sample preparation and thus a small difference in peak simulated and peak measured temperature is expected.

However, during the cooling cycle, there is a considerably large difference between simulated and measured temperatures of each duty cycle. In the developed LTspice welding model in Figure 10, the thermal properties of the materials were considered constant for the entire temperature range. However, in the case of polyethylene, the thermal properties of the material vary at a greater magnitude. A relative change in thermal properties of polyethylene between 20°C to 200°C from Shi *et al.* [11], is reproduced here in Figure 26. It shows that thermal properties are not constant and that there are large variations near the melting point, i.e. 125°C in the case of polyethylene. As the cooling phase was much longer than the heating phase, this effect was more significant in the cooling phase. To obtain thermal resistance and thermal capacitance values to build a Cauer RC-ladder, the thermal response curve of a system is normally either measured or simulated using the finite element method (FEM) [23]. These measured or simulated thermal response curves are then used to estimate the values of thermal resistance and thermal capacitance by using curve fitting [24]. The mathematical representation of the Cauer RC-ladders is very complicated and it is difficult to determine thermal parameter values by curve fitting [23]. The method adopted in this article utilizes the calculation of thermal parameters from the geometric shape and properties of materials. This type of Cauer RC ladder is easy to develop, has less complexity, and requires some compromise on transient thermal behavior [19].

In Akram *et al.* [17] it was shown that the cooling curve response depends on the calculated values of thermal resistance, thermal capacitance, and the values of convection resistance. For optimization of convection resistances, if Riconv and Roconv values are set to 45 ohms in the welding model shown in Figure 13, the results will look as shown in Figure 27. It can be easily observed that changing Riconv and Roconv values to 45 ohms has slightly increased the rate of the fall of the cooling curve (sim.opt-o200u, green curve), but it still does not match the measured cooling curve (meas-o200u, black curve) perfectly. With 45 ohms Roconv and Riconv, the power input to the OFEF joint with a 70% duty cycle will be slightly decreased to 31.81V $\times$ 5.49A $=$ 174.63 joules instead of 176.62 joules in Table 2. Due to a minor difference of 2 joules, the input power comparison will look very similar to the power comparison shown

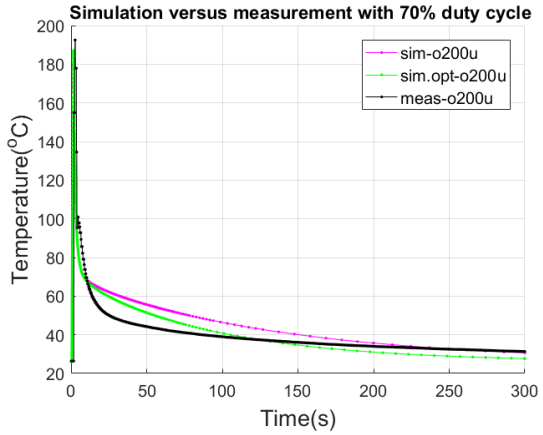

FIGURE 27. Result of optimizing Riconv and Roconv to 45 ohms on measured and simulated temperature of the OFEF joint with a 70% duty cycle.

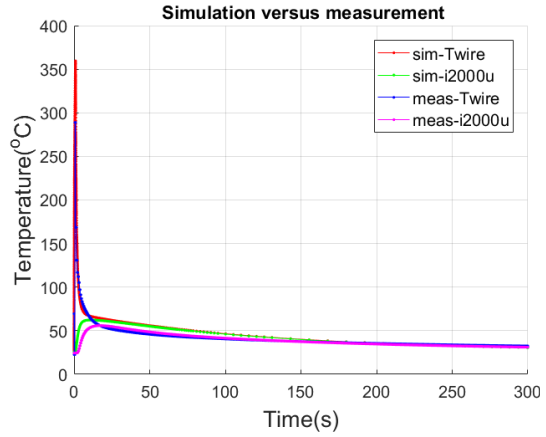

FIGURE 28. Comparison of simulated and measured wire and inner surface temperatures of a microduct with a 70% duty cycle.

in Figure 19 (a). A similar trend in power input and thermal response comparison can be observed with a simulation result of a 30% and 50% duty cycle for optimized Riconv and Roconv values of 45 ohms each.

Similarly, Figure 28 shows a comparison of simulated and measured wire temperature, as well as inner surface temperature of the microduct at layer Li2000 with a 70% duty cycle for the welding model in Figure 13. The measured wire temperature is 70°C lower than the simulated temperature, while the difference in the measured inner surface temperature of the microduct at layer Li2000 is within an acceptable range. This difference can be due to the sample and measurement tolerances discussed earlier. For example, if an attempt is made to match the simulated wire temperature to the actual measured wire temperature by increasing the Rthwire value in the welding model in Figure 13, then the node voltages of all following nodes become much lower than their present values, and a multiplication factor will be required to match the temperature at all the nodes. The optimization of wire temperature will require all the calculated thermal parameters to be changed due to the structure of the Cauer RC ladder and was thus ignored.

The calculated thermal parameters of the welding model in Figure 10 or 13 can be rationally varied by changing the values of variables X, Y, Z, and K. Despite the best efforts, the mismatch of thermal comparisons do not improve as required. It seemed like the transient capacitor discharge rate in LTspice was slower than the real measured discharge rate of electrical and thermal capacitances in this study. This might be one of the possible reasons behind the mismatch in comparisons of Figure 19 and 20.

In validation experiments, the thermal response time of thermocouple is dependent on its bead size [20]. The use of thicker or thinner thermocouples would have resulted in a different cooling curve. In real practice, OFEF joints are air-cooled through natural convection, depending on the temperature of the surrounding air and air velocity at the time of welding. Due to these uncertainties, the optimization of the thermal model was omitted and the calculated welding model of Figure 10 was considered sufficient for the development of a complete welding system. The developed welding model in Figure 10 is a purely theoretical model without any optimization involved. The developed welding model in Figure 10 tries to achieve a balance between simulated input power waveforms and the resulting thermal response. The advantages are that it is simple, has a very fast response time with DC step input (Figure 13), and can model the peak temperature on each layer of the OFEF joint simultaneously.

Results of measurement in Figure 19 and 20 are valid for only new joule heating wire that has never been subjected to joule heating before. Experiments have shown that joule heating the same wire for a second time has measured lower peak temperature compared to first time measured peak temperature. After a first time joule heating of copper wire, its resistance increased and its insulation was damaged, which resulted in lower temperature inside the surrounding LDPE layers.

From the results presented in Figure 19, and 20 it can be concluded that the welding model works well for the estimation of peak temperature inside the different layers of the OFEF joint for desired duty cycles. The welding model in Figure 10 can be used to compute the power consumption and resulting temperatures for the OFEF joint. Hence, all three temperature requirements set by Fujikake *et al.* [12] are met in the welding of the OFEF joint with a 70% duty cycle.

C. RESULTS OF PWM AND CAPACITOR BANK

A capacitor bank of 0.0562 farad was used to achieve higher than 160 watts of power effect with a 40 volts 4 ampere-hour battery, but it comes at a cost of higher losses during charging and discharging of the capacitor bank. However, this technique is very useful to increase the power level during the initial 100 milliseconds of the heating cycle. The capacitor bank was always charged at a 16% duty cycle with a charging frequency of 80 kHz in order to reduce the load on the battery. The current drawn from the battery during the charging of

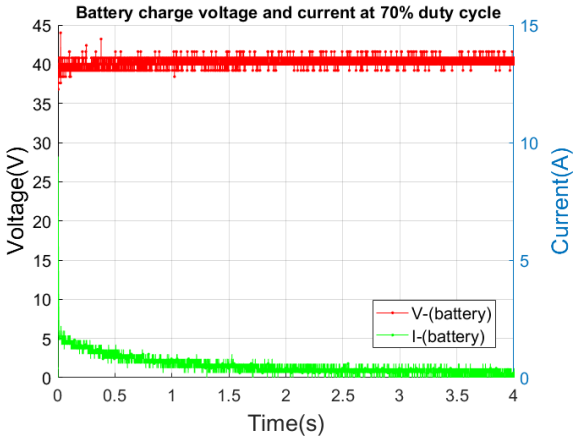

FIGURE 29. Voltage and current drawn from battery at a 16% duty cycle during charging of capacitor bank from 100 millivolts to 35 volts.

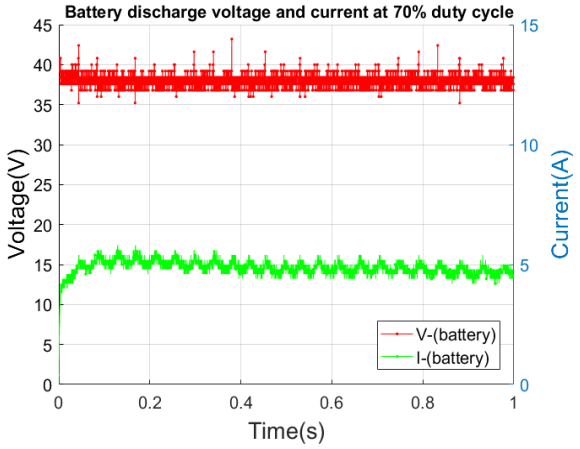

FIGURE 30. Voltage and current drawn from battery at a 70% duty cycle during welding with fully charged capacitor bank.

the capacitor bank from 100 millivolts to 35 volts is shown in Figure 29. It can be seen that current drawn from the battery at the start of the charging cycle has a maximum of around 2.5 amperes and gradually decreases as the capacitor bank charges to full capacity. The charging of the capacitor bank consumed $40.0 \times 0.5454 \times 4 = 87.27$ joules. The power drawn from the battery during welding with a 70% duty cycle, and with a fully charged capacitor bank, is shown in Figure 30. The discharge at a 70% duty cycle consumed $38.2 \times 5.24 = 200.16$ joules. The energy dissipated inside the OFEF joint was 167.74 joules, and the total energy loss was around 91.33 joules for the first weld. It is important to note that the capacitor bank was not fully discharged and 28.36 joules remained unused in the capacitor bank for the next welding. The energy loss for the second and following welding cycles was around 40 joules per weld due to the lower energy required to recharge the capacitor bank. If only a single weld is performed, the energy loss of the remaining 28.36 joules inside the capacitor bank can be avoided with software programming. The remaining energy may be totally consumed across the OFEF joint by turning off the charging MOSFET earlier than the one-second discharge time while keeping the discharge MOSFET turned on until the capacitor bank is completely discharged. The welding model shown in Figure 10 can be useful for finding and setting charge and discharge time. From the results in Figures 19, 26 and 27, it is obvious that a capacitor bank of 0.0562 farads can reduce the initial load on the battery, and provide a maximum of 196.1 joules of energy for the OFEF joint welding. The use of PWM is necessary to control the heat inside the OFEF joint to avoid overheating so that only the desired power is applied to the OFEF joint and thermal damage to the optical fiber microduct structure is avoided.

D. RESULTS OF THE LAYER MELT TEST

The layer melt test shown in Figure 21 shows that for a 70% duty cycle, heat penetrates for a maximum up to 400μm inside the optical fiber microduct, and the duct structure is not damaged during welding. It was also observed that only the sides of tightly wounded joule heating wire provided the strength for the OFEF joint. This verified the concept of increased joint strength as a result of the splitting of a single set of 14 turns joule heating wire into two sets of 7 turns each.

E. RESULT OF THE PULL STRENGTH TEST

For a compliance test with specifications of a mechanical joint, the pull strength and air pressure leakage test were performed on welds of 30%, 50%, and 70% duty cycle. For this purpose, each welded OFEF joint was pulled up to 300 newtons and then tested for air pressure leakage at 10 bars. The results of the pull strength test are presented in Table 3. The results show that a pull force of up to 300 newtons was unable to break the weld performed with each duty cycle. When the weld samples were pulled above 300 newtons, relative elongation was observed before the shear breakage of the OFEF joint wall above 400 newtons for each duty cycle. Based on the results shown in Table 3, it can be concluded that the pull strength of the LDPE joints is strong enough to replace mechanical joints.

F. RESULT OF THE AIR LEAKAGE TEST

After a non-destructive pull strength test of up to 300 newtons, each OFEF joint sample with 30%, 50%, and 70% duty cycle was tested for non-destructive air pressure leakage. Due to insufficient compressor pressure and lack of standard testing equipment, the air pressure damage and air leakage tests were only performed up to 10 bars on OFEF joints. Despite full effort, it was impossible to stop small leakages between the test sample and test equipment, due to the nozzle and pipes involved, as shown in Figure 23. For a standard comparison, a destructive air pressure test similar to the one performed by Majid *et al.* [25] on HDPE pipes, is required. The results of non-destructive, air pressure leakage tests are presented in Table 4. It can be seen that OFEF joints with 50% and 70% duty cycles had no leakage up to 10 bars. When

TABLE 3. Comparison of OFEF joint pull strength.

Duty Cycle	Pass	Fail
30%	≥300 newtons	-
50%	≥300 newtons	-
70%	≥300 newtons	-

TABLE 4. Comparison of OFEF joint air pressure test.

Duty Cycle	Pass	Fail
30%	-	≤1 bars
50%	≥10 bars	-
70%	≥10 bars	-

mechanical joints were tested for comparison, they showed leakage at less than 1 bar.

In the case of a welded OFEF joint, if it can pass 10 bars of air pressure with no leakage, there is no chance of water seepage inside it. Hence, the water seepage test was omitted. As previously mentioned, inside mechanical joints the air pressure and water seepage are solely dependent on the O-rings at both ends of the joint. The O-rings provide insufficient protection from air leakage and water seepage, therefore welding of optical fiber microducts was proposed and investigated in this article. The welded OFEF joints are far better than mechanical joints for air leakage and water seepage in this regard. When the layers of the OFEF joint and optical fiber microduct are welded together, a permanent melted bond is made with no risk of air leakage and water seepage. With no air pressure leakage, it is also possible to blow optical fibers for longer distances as compared to mechanical joints. This is a significant advantage of the developed OFEF joint welding system over traditional mechanical joints.

G. OXIDATION PROBLEM IN OFEF WELDING

In the development of the battery powered OFEF joint welding system, the presence of an oxide layer in the outer surface of microducts was ignored. However, in water and gas applications, the presence of oxidation in the outer surface layer is a major factor affecting the strength of the EF welding system [6], [11]. To overcome oxidation problems, manufacturers often use ultraviolet stabilizers [26], or sometimes peeling tools, to remove the thin outer surface layer of pipes before EF welding [27]. A sufficient outdoor exposure time, usually in the range of 3-12 months, is necessary, to induce oxidation on the outer surface of water and gas pipes, which can cause a significant decrease in the weld strength of the EF joint [16].

In the test performed by Shi *et al.* [15], it was observed that the joints with an oxidation layer tend to break at the fusion interface between the joint and pipe where the oxidation layer is present. If the oxidation layer is removed by a peeling or scraping tool, the joint will break in the area between the joule heating wires, which is the next weakest place in the EF joint [15]. In the more than 24 welding experiments performed for this article, there was not a single case of a poor quality joint in any of the test welds for each duty cycle. Before welding, no cleaning with any type of cleaning chemicals [27] was performed in any of the welding experiments. The OFEF joint welds were performed on more than 4-year-old optical fiber microducts, kept inside a lab room with sufficient electrical lighting, and a temperature range between 25°C-30°C. The exposed relative humidity level was as high as 50% during this period. No Fourier-transform infrared (FTIR) spectroscopy or ultraviolet absorption spectroscopy test [16] for oxidation level was performed on the optical fiber microducts used for the welding samples. Thus, the oxidation level of the optical fiber microducts was unknown for all the samples used for welding and tests. No information was available about the type of ultraviolet stabilizers, whether they were present or not, in the microduct samples used for welding.

TABLE 5. Comparison of OFEF joint and mechanical joint.

Test Property	OFEF Joint	Mechanical Joint
Dimeter	16.0 mm	32.0 mm
Length	34.0 mm	82.0 mm
Weight	1.50 grams	21.50 grams
Pull strength breakage	≥300 newtons	≥200 newtons
Air pressure damage	≥10 bars	≥15 bars
Air pressure leakage	≥10 bars	≤ 0.5 bars
Water seepage	No	No
Installation time	1-3 seconds	5-15 seconds
Assembly	1 piece	9 pieces

In tests performed by Allen *et al.* [16], an approximate decrease of 50% in EF joint strength was measured between a fresh gas pipe and a 12-month naturally UV exposed unscraped gas pipe, kept on the earth's surface. For a similar case in optical fiber microducts, by increasing the area of the heating zone and increased power supplied to the OFEF joint the effect of oxidation can be either eliminated or minimized and acceptable strength of the OFEF joint weld can be achieved. However, this needs to be further investigated. A summary of the comparison between the developed OFEF joint and the mechanical joint is presented in Table 5. The results in Table 5 show that the OFEF joint has a clear edge over mechanical joints. Because the oxidation problem was ignored in this study, welding with the highest possible duty cycle of 70% is recommended for a good quality OFEF joint weld.

V. CONCLUSION AND FUTURE WORK

Based on the results, it can be concluded that the developed optical fiber electrofusion joint and the battery powered welding system can replace the use of mechanical joints for fresh

or stored optical fiber microducts that are kept indoors, safe from ultraviolet exposure and water-induced oxidation. The developed optical fiber electrofusion joints are better than mechanical joints because less time is required per joint, their smaller size, lower weight, no air pressure leakage, and no water seepage qualities. For higher joint strength, it is recommended to manufacture the developed optical fiber electrofusion joint with injection molding techniques. The study lacks the welding of ultraviolet exposed, water submerged, and old buried optical fiber ducts, but it can be carried out in the future if needed. In such a case, the developed welding model may be utilized for deeper, stronger welds, or the usual oxidation removal methods and treatments developed for water and gas electrofusion welding can be adopted.

REFERENCES

[1] W. Griffioen, "The installation of conventional fiber-optic cables in conduits using the viscous flow of air," *J. Lightw. Technol.*, vol. 7, no. 2, pp. 297–302, Feb. 1989, doi: 10.1109/50.17770.
[2] A. Frank, G. Pinter, and R. W. Lang, "Prediction of the remaining lifetime of polyethylene pipes after up to 30 years in use," *Polym. Test.*, vol. 28, no. 7, pp. 737–745, Oct. 2009, doi: 10.1016/j.polymertesting.2009.06.004.
[3] S. Hornung, S. Cassidy, P. Yennadhiou, and M. Reeve, "The blown fiber cable," *IEEE J. Sel. Areas Commun.*, vol. 4, no. 5, pp. 679–685, Aug. 1986, doi: 10.1109/JSAC.1986.1146387.
[4] V. A. Burdin, T. G. Nikulina, I. N. Alekhin, and S. A. Gavryushin, "Researches of optical cable stability in the microduct to effect of freezing water," *Proc. SPIE*, vol. 7992, Apr. 2010, Art. no. 79920K, doi: 10.1117/12.887316.
[5] K. Mistry, "Tutorial plastics welding technology for industry," *Assem. Autom.*, vol. 17, no. 3, pp. 196–200, Sep. 1997, doi: 10.1108/01445159710172210.
[6] M. Troughton, *Handbook of Plastics Joining*, 2nd ed. Norwich, NY, USA: William Andrew, 2015, pp. 106–110, 360–368, 520, 525, and 529.
[7] J. Vlachopoulos and D. Strutt, "Basic heat transfer and some applications in polymer processing," in *Plastics Technician's Toolbox*, vol. 2. Brookfield, CT, USA: Society of Plastic Engineers, 2002, pp. 21–33.
[8] A. Zehtabeyazdi, S. M. Zebarjad, S. A. Sajjadi, and J. Abolfazli Esfahani, "On the sensitivity of dimensional stability of high density polyethylene on heating rate," *Exp. Polym. Lett.*, vol. 1, no. 2, pp. 92–97, 2007, doi: 10.3144/expresspolymlett.2007.16.
[9] J. Bowman, "A review of the electrofusion joining process for polyethylene pipe systems," *Polym. Eng. Sci.*, vol. 37, no. 4, pp. 674–691, Apr. 1997, doi: 10.1002/pen.11712.
[10] G. F. Rosala, A. J. Day, and A. S. Wood, "A finite element model of the electrofusion welding of thermoplastic pipes," *Proc. Inst. Mech. Eng., E, J. Process Mech. Eng.*, vol. 211, no. 2, pp. 137–146, May 1997, doi: 10.1243/0954408971529629.
[11] J. Shi, J. Zheng, W. Guo, P. Xu, Y. Qin, and S. Zuo, "A model for predicting temperature of electrofusion joints for polyethylene pipes," *J. Pressure Vessel Technol.*, vol. 131, no. 6, pp. 303–313, Dec. 2009, doi: 10.1115/1.4000202.
[12] M. Fujikake, M. Fukumura, and K. Kitao, "Analysis of the electrofusion joining process in polyethylene gas piping systems," *Comput. Struct.*, vol. 64, nos. 5–6, pp. 939–948, Sep. 1997, doi: 10.1016/S0045-7949(97)00008-4.
[13] S. Mansouri and M. S. Tavallali, "Heat transfer approximate modeling, parameter estimation and thermography of thermal pulsing in electrofusion joints of gas pipelines," *Infr. Phys. Technol.*, vol. 98, pp. 354–363, May 2019, doi: 10.1016/j.infrared.2019.03.002.
[14] M. Doaei and M. S. Tavallali, "Intelligent screening of electrofusion-polyethylene joints based on a thermal NDT method," *Infr. Phys. Technol.*, vol. 90, pp. 1–7, May 2018, doi: 10.1016/j.infrared.2018.01.030.
[15] J. Shi, J. Zheng, W. Guo, and Y. Qin, "Defects classification and failure modes of electrofusion joint for connecting polyethylene pipes," *J. Appl. Polym. Sci.*, vol. 124, no. 5, pp. 4070–4080, Jun. 2012, doi: 10.1002/app.35013.
[16] N. S. Allen, S. J. Palmer, G. P. Marshall, and J. Luc-Gardette, "Environmental oxidation processes in yellow gas pipe: implications for electrowelding," *Polym. Degradation Stability*, vol. 56, no. 3, pp. 265–274, Jun. 1997, doi: 10.1016/S0141-3910(96)00148-6.
[17] S. Akram, K. Bertilsson, and J. Siden, "LTspice electro-thermal model of joule heating in high density polyethylene optical fiber microducts," *Electronics*, vol. 8, no. 12, p. 1453, Dec. 2019, doi: 10.3390/electronics8121453.
[18] A. F. Robertson and D. Gross, "An electrical-analog method for transient heat-flow analysis," *J. Res. Nat. Bur. Standards*, vol. 61, no. 2, p. 105, Aug. 1958, doi: 10.6028/jres.061.016.
[19] Z. Wang and W. Qiao, "A physics-based improved cauer-type thermal equivalent circuit for IGBT modules," *IEEE Trans. Power Electron.*, vol. 31, no. 10, pp. 6781–6786, Oct. 2016, doi: 10.1109/TPEL.2016.2539208.
[20] Y. A. Cengel, *Heat Transfer A Practical Approach*, 2nd ed. New York, NY, USA: McGraw-Hill, 2003, p. 69, and 129-130,146-147,214,234-235,839.
[21] Y. Moumouni and R. Jacob Baker, "Concise thermal to electrical parameters extraction of thermoelectric generator for spice modeling," in *Proc. IEEE 58th Int. Midwest Symp. Circuits Syst. (MWSCAS)*, Aug. 2015, pp. 1–4, doi: 10.1109/MWSCAS.2015.7282014.
[22] Z. Chebbo, M. Vincent, A. Boujlal, D. Gueugnaut, and Y. Tillier, "Numerical and experimental study of the electrofusion welding process of polyethylene pipes," *Polym. Eng. Sci.*, vol. 55, no. 1, pp. 123–131, Jan. 2015, doi: 10.1002/pen.23878.
[23] Y. C. Gerstenmaier, W. Kiffe, and G. Wachutka, "Combination of thermal subsystems by use of rapid circuit transformation and extended two-port theory," *Microelectron. J.*, vol. 40, no. 1, pp. 26–34, Jan. 2009, doi: 10.1016/j.mejo.2008.09.002.
[24] J. Li, A. Castellazzi, M. A. Eleffendi, E. Gurpinar, C. M. Johnson, and L. Mills, "A physical RC network model for electrothermal analysis of a multichip SiC power module," *IEEE Trans. Power Electron.*, vol. 33, no. 3, pp. 2494–2508, Mar. 2018, doi: 10.1109/TPEL.2017.2697959.
[25] F. Majid and M. Elghorba, "HDPE pipes failure analysis and damage modeling," *Eng. Failure Anal.*, vol. 71, pp. 157–165, Jan. 2017, doi: 10.1016/j.engfailanal.2016.10.002.
[26] N. S. Allen, G. P. Marshall, C. Vasiliou, L. M. Moore, J. L. Kotecha, J. Luc-Gardette, and B. Valange, "Oxidation processes in blue water pipe," *Polym. Degradation Stability*, vol. 20, nos. 3–4, pp. 315–324, Jan. 1988.
[27] Y. Higuchi, H. Nishimura, F. Inoue, T. Ishikawa, and S. Miyaki, "Estimation of cooling time of electrofusion jointing in PE pipes for gas Distribution.," *Seikei-Kakou*, vol. 11, no. 9, pp. 795–800, 1999, doi: 10.4325/seikeikakou.11.795.

SHAZAD AKRAM received the M.Sc. degree in electronics from the Royal Institute of Technology, Stockholm, Sweden, in 2003. He is currently pursuing the Ph.D. degree with Mid Sweden University, Sundsvall, Sweden. He has worked many years in electro medical and electronics industry, as an Embedded Engineer and ATE Test Engineer. His interests include electronics system design, automated system testing, and system validation. Most recently, he has developed interest in thermal modeling and polymer welding.

JOHAN SIDÉN (Member, IEEE) received the M.Sc. degree in telecommunication, the Licentiate of Technology degree in electronics, and the Ph.D. degree in electronics from Mid Sweden University, Sundsvall, Sweden, in 2000, 2004, and 2007, respectively. He is currently an Associate Professor with Mid Sweden University. His current research interests include radio-frequency identification technology, wireless sensor networks, antenna technology, printed passive electronic systems, and optical fiber installation systems.

JIATONG DUAN received the B.S. degree in electrical engineering and automation from Beijing Information Science and Technology University, China, in 2018, and the M.Sc. degree in electronics from Mid Sweden University, Sweden, in 2020. She is currently a Test Engineer with Sanmina-Sci AB, Sweden, involved in the design, development, and implementation of testing systems. Her research interests include design automation, signal processing, and embedded systems.

MUHAMMAD FARHAN ALAM received the B.S. degree in electronics from Air University, Islamabad, Pakistan, in 2007, and the M.S. degree in electronics from Mid Sweden University, Sundsvall, in 2012. From 2012 to 2016, he worked as a Design Engineer with SEPS Technologies AB, Sundsvall, Sweden, during this time he worked with high frequency GaN power converters and designing electronic marker locator. Since 2016, he has been a Research Assistant with the Power Electronics Group, Mid Sweden University. His research interests include the development of a microcontroller system designing PCB for power converters testing and characterization of power converters.

KENT BERTILSSON (Member, IEEE) received the M.Sc. degree in electronics from Mid Sweden University, Sundsvall, Sweden, in 1999, and the Ph.D. degree from the Royal Institute of Technology, Stockholm, Sweden, in 2005, in the field of device design and optimization of silicon carbide devices. Since 2005, he has been leading the research in power electronics with Mid Sweden University, where he is currently a Full Professor. In 2009, he co-founded SEPS Technologies AB, Sundsvall, where he is the CEO. He has authored or coauthored more than 60 papers in international journals and conferences in the fields of semiconductor device simulations, silicon carbide devices, detectors, power electronics, and optical fiber installation systems.